ISSN: 2157-7439
Journal of Nanomedicine & Nanotechnology
OPEN ACCESS Freely available online
Research Article

Hyaluronic Acid Coated and Poly-L-Lysine Functionalized Graphene Quantum Dots for CD44 Targeted Anti-Cancer Drug Delivery against Osteosarcoma

Khushboo Dutta[1,2], Saty Decakash Ahirwar[2], Vijay Kumar Thakur[3,4,5], Piyush Kumar Gupta[6]*, Sunita Nayak[1,2]*

[1]*School of Bio Sciences and Technology, Vellore Institute of Technology, Vellore 632014, Tamil Nadu, India*
[2]*Centre for Biomaterials, Cellular, and Molecular Theranostics, Vellore Institute of Technology, Vellore 632014, Tamil Nadu, India*
[3]*Biorefining and Advanced Materials Research Centre, Scotland's Rural College (SRUC), Kings Buildings, Edinburgh EH9 3JG, UK*
[4]*Department of Mechanical Engineering, School of Engineering, Shiv Nadar University, Noida – 201314, Uttar Pradesh, India*
[5]*School of Engineering, University of Petroleum & Energy Studies (UPES), Dehradun – 248007, Uttarakhand, India*
[6]*Department of Life Sciences, School of Basic Sciences and Research, Sharda University, Greater Noida 201310, Uttar Pradesh, India*

ABSTRACT

Due to less toxicity and strong fluorescence properties, graphene quantum dots, i.e., GQDs have been shown to play a promising role in drug delivery applications. Hyaluronic acid (HA), used as a targeting ligand in this drug delivery system, is a polysaccharide which interacts with the hyaluronan receptor that is, CD44. Poly-L-lysine (PLL), containing amine groups, can be efficiently conjugated to the hydrophobic substances with carboxyl moieties. In this study, a novel drug delivery system composed of GQD coated with HA and coupled with PLL has been designed as a potent theranostic candidate for osteosarcoma therapy for the targeted delivery of DNA intercalating drug doxorubicin (DOX) to cancer cells. The characterization studies for morphology, structural analysis, and optical properties were evaluated. The drug loading, drug release profile, and anti-cancer effect of the GQDs-HA-PLL-DOX were investigated. The GQDs being synthesized have relatively narrow size distribution, with a diameter less than 5 nm. The maximum loading efficiency of the drug was achieved at 66% and pH-responsive drug release achieved was as high as 50%. The in vitro results showed good biocompatibility of GQD-conjugates. Fluorescence microscopy assay showed a fast and marked uptake of the drug with the time course. Hence, this system finds potential applications for in vitro cell imaging and targeted cancer therapy.

Keywords: Graphene quantum dot; Osteosarcoma; Targeted delivery; Anti-cancer activity; Fluorescence

INTRODUCTION

Osteosarcoma (OS) belongs to the spectrum of familial cancer predisposition syndromes and is a malignant tumor producing osteoid tissue [1]. Since OS contains various lineages of differentiation and unusual variants, therefore, histopathologic appearance is diverse, resulting in its aggressive behaviour which frequently results in treatment failure. The life expectancy has been improved to 60-70 % with current multimodal treatment strategies [2, 3]. Current medical therapies involve both neoadjuvant (pre-operative) and adjuvant (post-operative) chemotherapies and surgical treatment. However, in some cases, surgical resection is accompanied with radiotherapy. The degree of tumor necrosis after neoadjuvant or presurgical chemotherapy defines the effectiveness of the chemotherapy treatment and is also considered as a prognostic marker in the case of OS [4]. The histologic response of the tumor to neoadjuvant chemotherapy is used to define or estimate the survival rate. Therefore, drugs for adjuvant or postsurgical chemotherapy regimen need to be selected on the absis of degree of tumor necrosis induced by neoadjuvant chemotherapy [5]. The major challenge associated with designing an effective treatment strategy is the formulation of a chemotherapy regimen based on individual risk of relapse [6]. Nano-based drug delivery systems (NDDS) have offered a vast improvement in drug loading, targeting, and efficacy in cancer treatments [7]. Arrays of carbon-based materials such as the carbon allotropes, fullerene, carbon nanotubes, and graphene have been widely used in biomedical areas as biosensors, imaging probes, and DDS [8–10].

***Correspondence to:** Dr. Sunita Nayak, School of Bio Sciences and Technology, Vellore Institute of Technology, Centre for Biomaterials, Cellular, and Molecular Theranostics, Vellore Institute of Technology, Vellore 632014, Tamil Nadu, India, E-mail:- sunita013@gmail.com

Received: 03-Dec-2022, Manuscript No: jnmnt-22-19363, **Editor assigned:** 05-Dec-2022, Pre QC No jnmnt-22-19363 (PQ), **Reviewed:** 19-Dec-2022, QC No: jnmnt-22-19363, **Revised:** 22-Dec-2022, Manuscript No jnmnt-22-19363 (R), **Published:** 29-Dec-2022, DOI: 10.35248/2157-7439.22.13.651.

Citation: Dutta K, Ahirwar SD, Thakur VK, Gupta PK, Nayak S (2022) Hyaluronic Acid Coated and Poly-L-Lysine Functionalized Graphene Quantum Dots for CD44 Targeted Anti-Cancer Drug Delivery against Osteosarcoma. J Nanomed Nanotech. 13: 651.

Graphene and graphene oxide, i.e., GO; have attracted research interest in drug delivery applications due to their physico-chemical properties. In addition to this, they possess single atomic-layered structure [11]. Functionalization of graphene and GO has resulted in the improvement in drug solubility, extension of the half-life of drugs, and reduction in their side effects [12]. Graphene quantum dots (GQDs) are regarded as the next generation of carbon-based nanomaterials for drug delivery applications, since they are less toxic and more hydrophobic in nature when compared to graphene, and additionally exhibit strong fluorescence [13,14]. GQDs possess relatively higher number of active functional groups on their surface, because of which they are considered effective carriers of drugs for simultaneous treatment and tracking of cancer cells [15]. In addition to this, the unique structural property of GQD leads to the acceleration of the efficacy of anticancer drugs which is otherwise suboptimal owing to drug resistance [16]. The nuclear accumulation, DNA cleavage activity, and cytotoxicity of drugs such as adriamycin or doxorubicin and cisplatin (cis-diamminedichloroplatinum) have been significantly enhanced by GQDs [17].

Furthermore, the DDS is designed in such a manner that it recognizes cancer receptors on the cell surface, thus inducing receptor-mediated endocytosis, and minimizing systemic toxicity, often associated with conventional chemotherapeutic approaches. Therefore, while designing DDS for targeted drug delivery, it is usually conjugated with a tumor-targeting ligand that recognizes receptors which are over-expressed on cancer cells [18]. Among the receptor binding molecules which have been widely reported, hyaluronic acid (HA) is extensively utilized as targeting ligand, owing to properties like biocompatibility, biodegradability, and minimal toxicity. HA can easily bind with exceptionally high affinity to the CD44 (hyaluronan) receptor that has been observed to be upregulated in cancers of epithelial origin. Moreover, cancer angiogenesis and tumor progression are linked with CD44 overexpression [19]. Though, healthy tissues also show the endogenous CD44 expression at low levels, which may result in side effects [20, 21]. The effective strategy for cancer treatment involves targeting drugs either to CD44, HA matrix or interactions between HA matrix and CD44 [20]. The CD44 isoforms possessing multiple cellular functions play a vital role in the pathogenesis of cancer. The CD44 isoforms are expressed at varying levels in different forms of cancer. CD44 expression is regulated by various signalling networks, transcriptional repressors and activators, epigenetic mechanisms, and miRNAs [22].Thomas et al in their study reported that paclitaxel-loaded HA Nano particulate micelles were an efficient chemotherapeutic treatment strategy for cancer cells showing CD44 overexpression [23]. The findings of Nahain et al. suggest that GQD can be efficiently used as a drug carrier and additionally, the in vitro cytotoxicity assay supports the fact that GQD-HA conjugate possesses high biocompatibility [24]. Stimuli-responsive hyaluronic acid-coated Nano medicines are extensively studied as potential agents for clinical cancer therapy [25]. Nigam et al in a study investigated hyaluronic acid-functionalized GQD-labelled human serum albumin (HSA) nanoparticles as a potent drug delivery system for the treatment of pancreatic cancer [26].

The amine groups in poly-L-lysine (PLL) can be chemically conjugated with carboxyl groups of hydrophobic substances, thus encapsulating lipophilic drugs. Therefore, cancer can be targeted and efficiently diagnosed by binding of the chemical moieties in the ligands with the amine groups [27]. Moreover, the conversion of an amine group of PLL into a positively charged hydrophilic amino group under acidic conditions, results in an electrostatic (non-covalent) interaction with the negatively charged membrane of cancer cell. PLL being a polycationic peptide can be selectively internalized into cancer cells through a mechanism involving electrostatically adsorptive endocytosis [28]. Graphene quantum dots covalently linked to tumor-targeting ligand, HA-PLL complex could be an effective strategy to achieve the targeted delivery of anti-cancer drug DOX for osteosarcoma therapy. The objective of this study was to design a new biocompatible Nano-drug delivery system, able to ensure the targeted delivery of drugs.

In the present work, highly water dispersible GQD, were synthesized using the electrochemical exfoliation method and were coated with tumor-targeting module HA and functionalized with Poly-L-lysine complex (GQD-HA-PLL).In this experimental work the size, morphology, structural analysis, optical properties, drug release kinetics, and biocompatibility of the GQD-HA-PLL complex were investigated.

MATERIAL AND METHODS

Materials

Solvents and reagents were purchased from commercial suppliers and were used without further purification. Graphite rods of purity >99.9995 % were purchased from Alfa Aesar (CAS No. 7782–42-5). Citric acid monohydrate (MW = 210.14 g/mol) and calcium chloride anhydrous (110.98 g/mol) were purchased from Himedia Laboratories (Mumbai, India). 1-Ethyl-3-(dimethylaminopropyl) carbodiimide (155.24 g/mol), N-hydroxysuccinimide (115.09g/mol), hyaluronic acid sodium salt, poly-L-lysine, doxorubicin hydrochloride, and 3-(4,5-dimethylthiazol-2-yl)-2,5-diphenyl tetrazolium bromide (MTT) was purchased from Sigma Aldrich (India) (Products were manufactured in the UK, Japan, and Germany). Sodium hydroxide (MW = 40.00 g/mol) was purchased from SD-Finechem Ltd. (Maharashtra, India).All solutions were prepared with ultra-pure water or 0.01M phosphate buffer saline (PBS, pH 7.4) unless otherwise specified.MG 63 cell lines were obtained from National Centre for Cell Science (NCCS), Pune. DMEM (Dulbecco's minimal essential medium), Foetal bovine serums(FBS), trypsin, and 1X antibiotic (Penicillin-Streptomycin) solution were purchased from Hi-Media Laboratories, Mumbai, India.

GQD Synthesis

GQDs were prepared by the electrochemical exfoliation method described by Ahirwar et al [29]. Briefly, the graphite rods were heated in a furnace at 1050°C for 5 min in the presence of air, followed by cooling at room temperature. This step was followed by washing the graphite rods with Milli-Q water. This step was done in order to remove the large particles from the surface of the rods. The graphite rods acted as anode and cathode. In an electrochemical experiment, anode and cathode are the electrodes which are dipped in the electrolyte solution. A mixture of citric acid monohydrate (0.1 M) and sodium hydroxide, i.e., NaOH (0.15-0.4 M) in 50 mL Milli-Q water was used as an electrolyte. Electrochemical workstation was used to carry out the experiment. The graphite rods were placed 25 mm apart. Cyclic Voltammetry (CV) was performed with a voltage ranging from -1 to +1 V. This was done in order to wet the graphite electrodes. This was followed by chrono-amperometry with a voltage of +10V for 30 min. This resulted in the change of the colour of the electrolyte solution to yellow, indicating the exfoliation of the graphite rod.

Calcium chloride (0.15 M) was then added to the solution after completion of the reaction, followed by heating the solution to precipitate calcium citrate. This step was followed by centrifugation for 15 min at 10,000 rpm. The centrifugation step was done twice in order to separate the precipitate, i.e., calcium citrate. The supernatant was then filtered through dialysis membrane filtration (dialysis membrane-60, cut-off 1,000 Da, Himedia Laboratories), consecutively for 7 days to remove the salt content from the solution with the repeated changes of distilled water.

Synthesis of GQD-HA-PLL

To a solution of GQD (0.3mg/mL),in PBS buffer pH 7.4 (10 mL)under stirring100 µL HA (1 mg/1 mL d/w) was added for 30 min. Afterward, 1-(3-dimethyl-aminopropyl)-3-ethylcarbodiimide hydrochloride (EDC) (96 mg) and N- hydroxysuccinimide (NHS) (11.5 mg) were added to the resultant mixture was allowed to react for 30 min at room temperature.To this mixture, 200 µL PLL (1 mg/1 mL d/w) were added and kept for overnight stirring. Hydroxylamine hydrochloride (10 mM) was added after 12 h for quenching the reaction. Solution was repeatedly dialysed against distilled water using dialysis membrane tubing for 24h (MW cut-off 1,000 kDa). Purified solution was stored at 4° C.

Synthesis of GQD-HA-PLL-DOX Conjugates

Model drug doxorubicin hydrochloride, 200 µL (DOX solutions) of different concentrations ranging from 100, 200, 300, 400 to 500 µg/mL was loaded on GQD-HA-PLL (1 mL of 0.3 mg/mL) in PBS solution, with continuous stirring for 24h in dark at room temperature. The mixture was centrifuged at 12,000 rpm for 30 min. Pellet was regarded as GQD-HA-PLL-DOX and free DOX content remained in the supernatant was estimated by taking absorbance at 480 nm [30].

PHYSICOCHEMICAL CHARACTERIZATION STUDIES

Transmission Electron Microscopy

Transmission electron microscopy (TEM, FEI – Tecnai G2 20 Twin) was employed to investigate the size and the surface morphology of the synthesized GQD nanoparticles (GQD NPs). TEM samples were prepared by placing the aqueous suspension of GQDs on the copper grids followed by drying under ambient conditions. Furthermore, dynamic light scattering (DLS; HORIBA SZ-100 Nanoparticle analyser; HORIBA Ltd.) was used to detect the particle size of GQDs.

Surface Charge and Hydrodynamic Size Analysis

Nanoparticle analyser (HORIBA SZ-100) was used to determine the average zeta potential (ζ-potential) and average hydrodynamic size values of the GQD. The measurements were done at a wavelength of 659nm and at an angle of 173° relative to the incident beam.

UV-Visible Spectroscopy

UV-Visible (UV-Vis) spectroscopy (JASCO-V-670 PC) was used to study the conjugation of GQDs to HA-PLL and to characterize their functional groups.

Fluorescence Spectroscopy

Fluorescence spectra (Excitation-dependent photoluminescence behaviour) were recorded using a Hitachi F-2500 fluorescence spectrophotometer. The GQDs and the conjugates were excited at a wavelength of 350 nm.

Raman Spectroscopy

The morphology of GQD and its conjugates was examined using Raman spectroscopy (Raman spectrophotometer (536 nm)-Agiltron, USA; with a power of 10 mW).

Drug Loading and Release Studies

During loading of the antitumor drug to GQD conjugates, the bath solution was changed every 4h. All bath solutions were collected, followed by measurement of absorbance at 480 nm to calculate the free drug content. The absorbance corresponding to the different concentrations of DOX, measured at 480 nm was normalized by linear regression. The loading efficiency of the drug, i.e., DOX was calculated using the following equation:

$$D_L = \left(\frac{w - w0}{W}\right) \times 100 \quad (1)$$

Where, D_L = loading efficiency (determined in %), w, w0 = weights of drug added and free drug, respectively, and W = weight of carriers

The percentage of DOX release was calculated using the following equation:

$$D_R = \left(\frac{w}{W}\right) \times 100 \quad (2)$$

Where, D_R = drug release (%), w = weight of free drug present in the supernatant, and W = weight of drug loaded in the system

Cell Culture

Cells (MG-63 cell line) cultured in a DMEM medium supplemented with 10 % fetal bovine serum (FBS) and 1% antibiotic (penicillin-streptomycin) in an atmosphere with 5% CO_2 and 37°C inside a CO_2 incubator. The cells, after attaining 90% confluence, were harvested from cell culture flasks and were suspended in a fresh complete medium before plating.

Cell Viability Assay

The in vitro-cytotoxicity of free GQDs, GQD-HA-PLL, and GQD-HA-PLL-DOX was evaluated by MTT (3-(4, 5-dimethylthiazol-2-yl)-2, 5-diphenyl tetrazolium bromide) assay which is used to determine the cell viability, by a protocol described by Wang et al [39]. Briefly, the cells were seeded on 96-well plates at 2x 10^4 cells/well in 100 µL of complete medium. The plates were incubated for 24h at 37°C in a humidified 5% CO_2 atmosphere, followed by incubating the cells (except control), with incomplete media (DMEM) for 2h for facilitating the cellular uptake process. After 2h, incomplete media was discarded and, the cells were incubated with a fresh medium containing GQD (33.7 µg/mL), GQD-HA-PLL (33.7 µg/mL) or GQD-HA-PLL-DOX (33.7 µg/mL), for 24h and 72h, respectively. The wells containing cells without GQDs, GQD-HA-PLL or GQD-HA-PLL-DOX, served as the control. After a time period of 24h and 72h, culture liquid from samples was discarded from the wells and 100 µL MTT (0.5 mg/mL in PBS) was added to each well and incubated for 4h. Later the solution was discarded from each well and 100 µL DMSO was added to each well in order to dissolve formazan crystals. The absorbance of each sample at 570 nm was measured using a spectrophotometer (Readwell TOUCH, ROBONIK, and India).

The cell viability ratio was calculated using the following equation:

$$\text{Cell viability (\%)} = \left(\frac{A}{A0}\right)\times 100 \quad (3)$$

Where, A = absorbance (or optical density) of the sample (at 570 nm) and A0 = absorbance (or optical density) of control (at 570 nm)

Fluorescence Microscopy Analysis

MG-63 cells were used to verify the selective uptake of GQD-conjugates. For the drug delivery assay, as described by Wnag et al, the cells at a density of $2x10^4$ per well were seeded in a 96-well plate and cultured for 24h, subsequently starved with DMEM medium for 2h, and then incubated with GQD (33.7 µg/mL), GQD-HA-PLL (33.7 µg/mL) or GQD-HA-PLL-DOX (33.7 µg/mL), containing DMEM supplemented with 10% FBS for 24h. Cells cultured in the medium without GQDs were taken as the control [39]. After incubation (24h), the fluorescence of cells was observed using a fluorescence microscope at the excitation of 405 nm (ZEISS Axio Observer Research Inverted Microscope, Bio compare).

Statistical Analysis

Statistical analysis was performed using Graph Pad Prism Software (Chicago. IL, USA). All experiments were performed in triplicates for at least three independent times. All mean values are presented with the standard deviation. One-way analysis of variance (ANOVA) was used to analyze the corresponding treatment effcets. Significance between groups has been analysed using the student's t-test ($p < 0.0001$).

RESULTS AND DISCUSSION

Synthesis Of Gqds And Gqd-Ha-Pll-Dox Conjugates

The strategy of synthesis of GQDs by electrochemical exfoliation method was followed according to the procedure described by Ahirwar et al. as shown in Figure 1. The GQDs were prepared by the electrochemical exfoliation method, during which the processes of cutting and oxidation occur at the defect sites. This technique of synthesis utilizes two graphite rods as electrodes and a mixture of citric acid and sodium hydroxide as electrolytes. High-temperature heating of graphite rods generates defects on the surface. The sodium hydroxide in the electrolyte generates GQDs with oxygen-rich functional groups [29]. The GQDs formed using this method have an average size of 4.5 nm, with an interplanar spacing of 0.21 nm, with the lattice spacing in accordance with the graphene structure [29]. The photo luminescent properties of GQDs were exploited to monitor the cellular uptake process in vitro, as evident in the fluorescence microscopy assay. GQDs were coated with HA and functionalized with PLL complex as the targeting ligand, in order to facilitate the uptake into the target cancer cells. GQDs' surface properties have a significant role in the conjugation process as it governs the attachment of biomolecules to their surface [31]. In this work prepared GQD were coated with HA and coupling reaction of PLL with coated GQD surface was done using, EDC/NHS as coupling agents. Covalent binding of several biomolecules using carbodiimide mediated coupling that exploits cross linking between amine and carboxylic functional groups [32]. The EDC crosslinking mechanism depends on the reaction with carboxyl groups of GQD/ or HA, that may react with the amino groups of PLL, resulting in the amide bond formation.

PHYSICOCHEMICAL CHARACTERIZATION STUDIES

Transmission Electron Microscopy

The representative TEM image (Figure 2a) of synthesized GQDs showed homogeneously distributed GQD nanoparticles with a diameter less than 5 nm. The semiconductor quantum dots and metal Nano-clusters which are most commonly used in various applications, are mainly spherical Nano-crystals with higher molecular weight (>30kDa) [33, 34, 39]. Usually, the size distribution of GQDs obtained through the electrochemical exfoliation method is in the range of 1.5 - 4.5 nm [29]. The lattice spacing in particles corresponds to the 100 hexagonal lattice spacing along the [001] direction, which is characteristic of that present in the graphene structure [35]. A higher drug loading capacity is achieved when GQD is used as a carrier, a property that can be attributed to the unique structure of GQDs resulting in a high surface-to-volume ratio [39].

Surface Charge And Hydrodynamic Size Analysis

Zeta potential measurement was done by SZ-100Horiba and the according to the result obtained, GQDs acquired a net negative surface charge of -22.1±3.66 mV. The average hydrodynamic size of GQDs was 4.5 nm, as measured by DLS (Figure 2b). The figure illustrates the macroscopic state of the GQD colloidal systems. Zeta potential signifies the dispersion stability of a sample. The higher the magnitude of zeta potential, the greater is the stability of the electrostatically stabilized suspension over a period of time. In principle, zeta (ξ) potential is a term used for the electro-kinetic potential present in colloidal dispersions; its magnitude indicates the extent of electrostatic repulsion between the particles in dispersion bearing similar charges and which are adjacent to each other. For the small-sized particles and molecules, higher values of zeta potential indicate that the dispersion will resist aggregation i.e., the solution is highly stable. On the other hand, in the case of smaller values, attractive forces may exceed the repulsion, which may ultimately lead to the breakage and flocculation of dispersion [36]. Therefore, the electrically stabilized colloidal solutions tend to

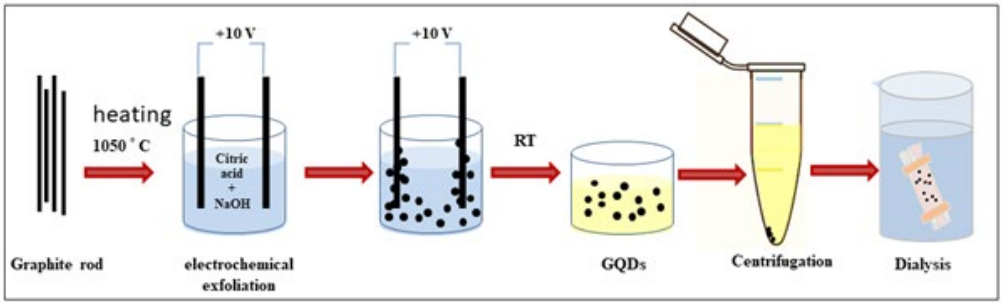

Figure 1: Schematic illustration of synthesis of GQDs.

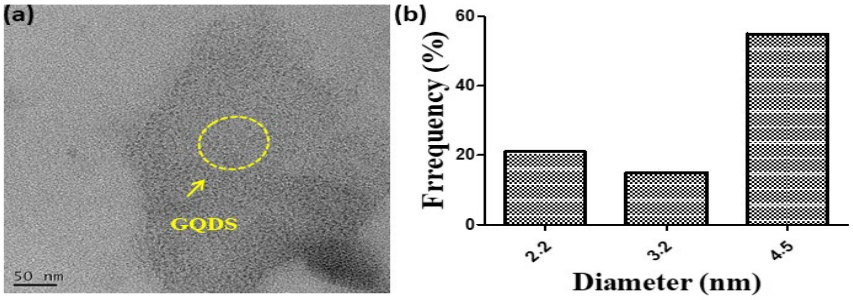

Figure 2: (a) TEM image of GQDs (Scale bar = 50 nm), (b) Particle size distribution of GQDs measured by DLS.

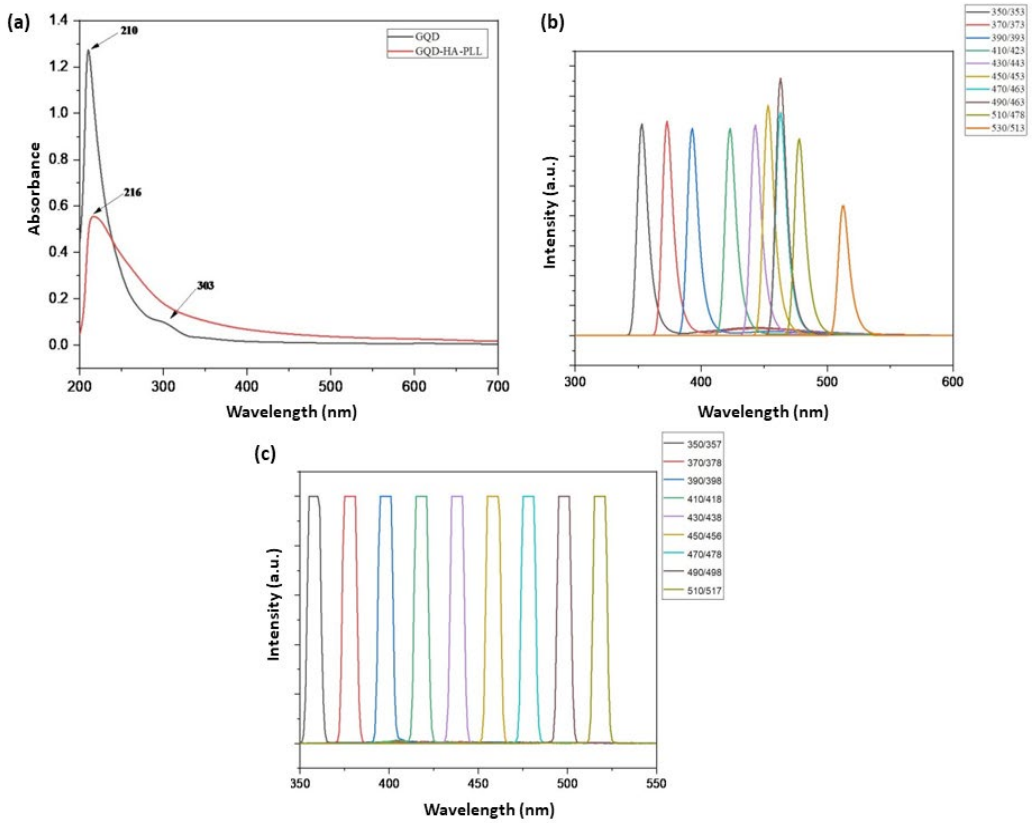

Figure 3: (a) UV-Visible spectra (b, c) Excitation-dependent Photoluminescence Behaviour of GQD and GQD-HA-PLL, Respectively.

have high zeta potential (negative or positive) values, while those with lower zeta potential values will have a propensity to coagulate or flocculate [36-37].

UV-Visible Spectroscopy

UV-Visible spectra of GQD and GQD-HA-PLL samples are illustrated in Figure 3a. In the UV-Visible spectra, two prominent peaks were observed at 210 and 303 nm in the case of GQDs. A new peak at approximately 216 nm appeared after the conjugation, which confirmed the functionalization of GQD with PLL, which concedes with the previous study done by Wang et al. [39]. Furthermore, the decrease in UV-visible absorbance indicated the interaction between GQDs and the targeting ligand. Generally, an absorption peak between 253 and 279 nm corresponds to the $\pi \rightarrow \pi^*$ transition of sp^2 hybridized C-C bonds, while a peak around 325-370 nm corresponds to the $n \rightarrow \pi^*$ transition [29, 38].

Excitation-Dependent Photoluminescence Behaviour

The excitation-dependent photoluminescence behaviour of GQDs and GQD-HA-PLL is shown in Figure 3b, c. GQDs exhibit photoluminescence properties primarily due to a phenomenon known as the quantum confinement effect which occurs due to the carbon core and, also the presence of functional groups on the surface giving rise to multiple surface states [38]. The presence of functional groups such as C-H, C-O, C=O, and O-C=O contributes significantly to the luminescence properties of GQDs [29]. The variation in the excitation wavelength ranging from 350 to 510 nm with an increment of 20 nm has been done and the corresponding emission wavelength was observed. A change in the emission wavelength has been observed with the variation of excitation wavelength. In the case of GQD, a reduction in the peak intensity of emission is observed as the excitation wavelength increases (Figure 3b). However, after functionalization of GQD with HA and PLL, no significant change in the peak intensity of emission is observed (Figure 3c).

Raman Spectroscopy

As shown in Figure 4a, two distinctive bands, in both the cases, are observed in the Raman spectrum of GQDs. In case of GQDs, the bands were observed at 558 cm^{-1} and 1092 cm^{-1} with an intensity ratio (I_D/I_G) of 0.46. While after the conjugation process, the corresponding peaks were obtained at 561 cm^{-1} and 1093 cm^{-1}

(Figure 4b), with an intensity ratio (I_D/I_G) being 0.42. The peak intensity ratio in Raman spectra is a measure of the crystallinity of prepared GQDs and also the uniqueness of electrochemical exfoliation method used for the preparation of GQDs [29, 40]. The G band is primarily due to E_{2g} phonon vibrations arising due to strains produced in the sp^2 hybridized carbon. Furthermore, the disorder present on the edges which may be in the form of sp^3 hybridized carbons, surface states, or functional groups on the surface of GQDs, is confirmed by one additional band, i.e., D band, often defined as a disorder-induced band, which arises due to bonding and anti-bonding orbitals [29]. Moreover, the broadening of D peak, in both the cases, as is evident in figure, is possibly due to an increase in sp^3 hybridized content in various functional groups involving carbon-carbon bonds (C-C), carbon-oxygen bonds (C-O, C=O), epoxy (-O-) and hydroxyl (-OH) moieties [29,41]. The intensity ratio of D band to G band (I_D/I_G) is defined as a measure of degree of disorder (or randomness) present in the system [29, 42]. The intensity ratio (I_D/I_G) is known to be inversely proportional to the crystalline grain, when described for the Nano-crystalline graphite [43].

Drug Loading And Release Studies

As is evident in Figure 5a, when the loading ratio of drug to nanoparticle targeting ligand conjugate, i.e., DOX to GQD-HA-PLL was 3:5, the maximum loading efficiency of DOX in GQD-HA-PLL was achieved, which was at 66%. The drug release behaviour of the drug delivery system was monitored in the cell culture medium at 24h. The release of drug (DOX) from GQD-HA-PLL could reach as high as 50%, as seen in Figure 5b. When the abiotic experiments were carried out on this drug delivery system, it confirmed the selective pH-triggered drug release mechanism and the results of these studies showed no significant drug release at neutral conditions (pH = 7.4). However, at pH = 5.5, a significant drug release was observed, which confirmed a selective pH-triggered drug release mechanism [32]. Thus, the GQD-HA-PLL-DOX drug delivery system (DDS) achieved a significant loading efficiency capacity in terms of DOX.

CELL CULTURE STUDIES

Cell Viability Assay

The first step of biological experiments generally aims to check the biocompatibility of the nanoparticle based drug delivery system [32]. The biocompatibility of GQD was assessed by MTT assay which determined the percent cell viability after treatment for 24h (Figure 6a) and 72h (Figure 6b) respectively. Cell viability, which is expressed as the percentage of viable cells in comparison to the untreated control cells, remained above 50% in both GQD and GQD-HA-PLL treated cells. However, in the case of DOX-loaded GQD conjugates, viability was significantly reduced, thus indicating that a GQD-based drug delivery system can efficiently target cancer cells (Table 1). These in vitro results validated the good biocompatibility of GQD-conjugates, and in addition to this, also suggested an enhanced active targeting efficiency against osteosarcoma (Ko et al., 2017). Cytotoxicity of GQDs can also be further assessed by performing the lactate dehydrogenase (LDH) release assay as the LDH level out of cells is a marker of cell membrane integrity (Jiang et al., 2015) [44].

Fluorescence Microscopy

Photoluminescence is one of the characteristic properties of GQDs

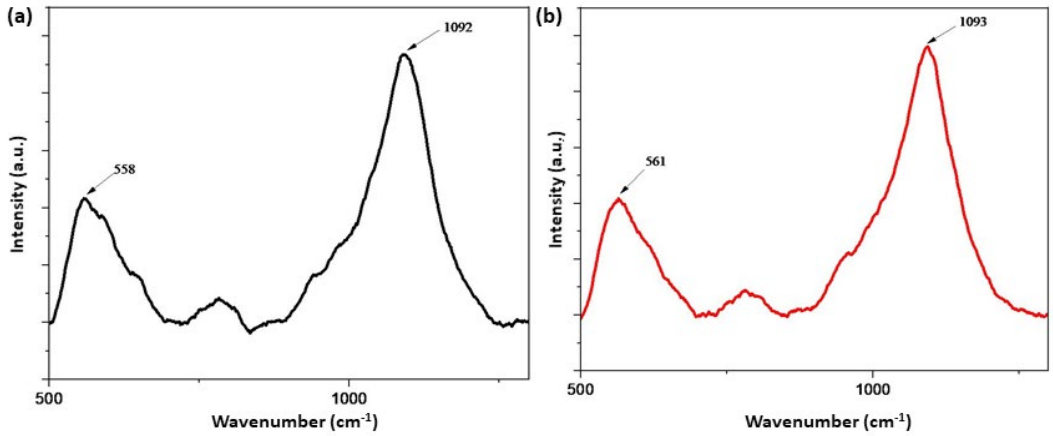

Figure 4: (a, b) Raman Spectra of GQD and GQD-HA-PLL, Respectively.

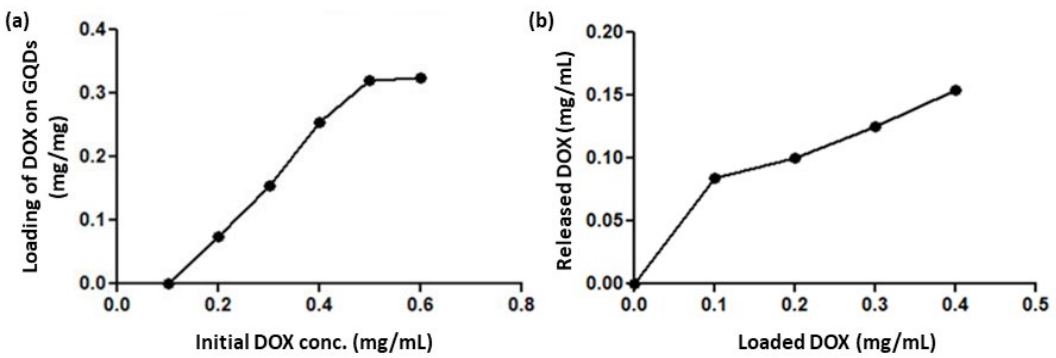

Figure 5: (a) Drug loadingand (b) release profiles of GQD-HA-PLL-DOX in aqueous solution.

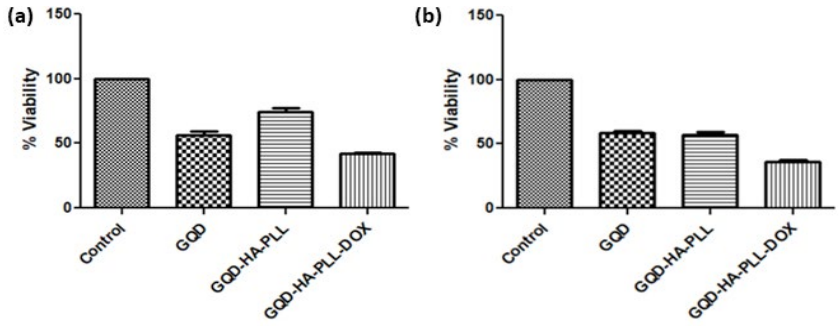

Figure 6: Cell viability assay carried out on MG-63 (osteosarcoma) cells for 24h (a) and 72h (b) using GQD, GQD-HA-PLL, and GQD-HA-PLL-DOX. The Resulting data were presented as Mean ± SD.

Table 1: Cell viability assay assessed after treatment for 24 and 72h, respectively. Expressed as a percentage of viable cells relative to the untreated (control) cells ($p < 0.0001$).

Experimental Groups	Cell viability (%) at 24h	Cell viability (%) at 72h
Control	100 ± 0.0	100 ± 0.0
GQD	56.74 ± 2.62	58.27 ± 1.64
GQD-HA-PLL	74.37 ± 2.78	57.21 ± 2.27
GQD-HA-PLL-DOX	42.06 ± 1.15	36.07 ± 1.87

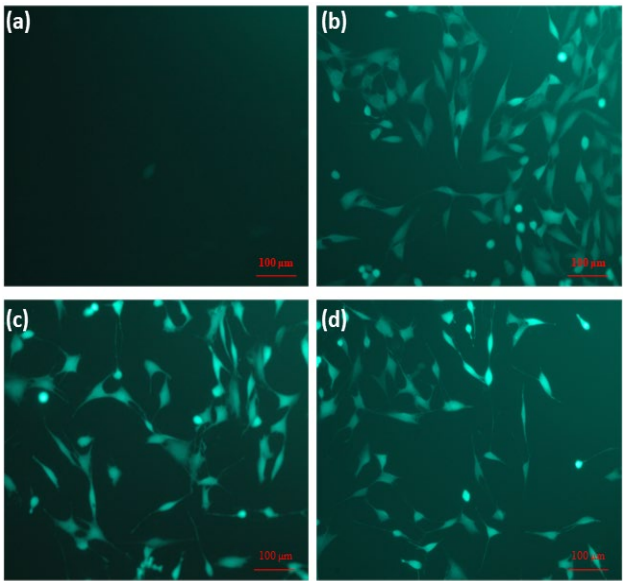

Figure 7: Fluorescence images of MG-63 cells (a) control cells, (b–d) treated with GQD, GQD-HA-PLL, and GQD-HA-PLL-DOX for 24h respectively(magnification 20X).

that makes them find potential applications in bio-imaging studies as probes [44]. The chemical nature of quantum dot surfaces can be easily modulated which makes them potent fluorescent bio-probes. GQDs have been reported to enter the cells through receptor-mediated endocytosis [30, 45]. The rate of internalization of GQDs varies with the size. For example, nano-sized GQDs could be internalized into cells faster when compared with the micro-sized GO sheets [16]. In the experiment, the prepared GQDs and conjugates emitted green luminescence, thus, they might be good candidates for fluorescent probes in cell imaging. As shown in the figure, the fluorescence microscopy images of the cells incubated with GQD and GQD-HA-PLL were brighter than those without GQD treatment (Figure 7a). The fast uptake of the drug was observed with the time course (Figure 7b-d). Thus, GQD-based drug delivery system is a promising candidate for targeted drug delivery in osteosarcoma treatment [46, 47].

CONCLUSIONS

In conclusion, a novel GQD-based nano-drug delivery system was designed for use as a promising theranostic agent for OS therapy. GQDs were prepared by the electrochemical exfoliation method and were further conjugated with hyaluronic acid (HA) and Poly-L-lysine (PLL). GQDs were grafted with hyaluronic acid (HA), which involved amide bond formation via the reaction between the amine (NH_2) groups of HA and COOH groups of GQDs [39]. GQDs exhibit bright fluorescence and excellent solubility in an aqueous solution, properties which enable them to be used for biomedical purposes. The GQDs-HA-PLL-DOX drug delivery system was successfully synthesized with a significant loading efficiency in terms of DOX. The in vitro studies validated the fact that GQDs possess low toxicity and thus, find great potential in biomedical applications. Moreover, their multimodal conjugation allows the incorporation of both, drugs and targeting ligands in the same nanostructure [32]. Therefore, the systemic toxicity induced by anticancer drugs and most often associated with conventional chemotherapy, is significantly minimized by this approach.

CONFLICT OF INTEREST

The authors declare no conflicts of interest.

ACKNOWLEDGEMENT

Authors wish to acknowledge VIT, Vellore for funding the research as “Seed Grant 2020-21”. Dr. Piyush Kumar Gupta is thankful to Department of Life Sciences, School of Basic Sciences and Research, Sharda University for the infrastructure and research facilities.

FUNDING

This research did not receive any specific grant from the funding agencies in the public, commercial, or not-for-profit sectors.

REFERENCES

1. Gaspar N, Di Giannatale A, Geoerger B, Redini F, Corradini N, Enz-Werle N, et al. Bone sarcomas: from biology to targeted therapies. Sarcoma. 2012; 14:96.

2. Ferguson W S, Goorin A M. Current treatment of osteosarcoma. Cancer investigation. 2001; 19(3) 292-315.

3. Rytting M, Pearson P, Raymond A K, Ayala A, Murray J, Yasko A W, et al. Osteosarcoma in preadolescent patients. Clinical Orthopaedics and Related Research. 2000; 373 39-50.

4. Bielack S S, Kempf-Bielack B, Delling G, Exner G U, Flege, S, Helmke K, et al. Prognostic factors in high-grade osteosarcoma of

the extremities or trunk: an analysis of 1,702 patients treated on neoadjuvant cooperative osteosarcoma study group protocols. Journal of clinical oncology. 2002; 20(3): 776-790.

5. Bacci G, Longhi A, Fagioli F, Briccoli A, Versari M, Picci P. Adjuvant and neoadjuvant chemotherapy for osteosarcoma of the extremities: 27 year experience at Rizzoli Institute, Italy. European Journal of Cancer. 2000; 41(18): 2836-2845.

6. Carrle D, Bielack S S. Current strategies of chemotherapy in osteosarcoma. International orthopaedics. 2006; 30(6): 445-451.

7. Liu D, Yang F, Xiong F, Gu N. The smart drug delivery system and its clinical potential. Theranostics. 2006; 6(9): 1306.

8. Iannazzo D, Piperno A, Pistone A, Grassi G, Galvagno S. Recent advances in carbon nanotubes as delivery systems for anticancer drugs. Current medicinal chemistry. 2013; 20(11): 1333-1354.

9. Iannazzo D, Pistone A, Galvagno S, Ferro S, De Luca L, Monforte A M, et al. Synthesis and anti-HIV activity of carboxylated and drug-conjugated multi-walled carbon nanotubes. Carbon. 2015; 82: 548-561.

10. Marchesan S, Prato M. Nanomaterials for (Nano) medicine. ACS medicinal chemistry letters. 2013; 4(2): 147-149.

11. Zhang Q, Nguyen A L, Shi S, Hill C, Wilder-Smith P, Krasieva T B, et al. Three-dimensional spheroid culture of human gingiva-derived mesenchymal stem cells enhances mitigation of chemotherapy-induced oral mucositis. Stem cells and development. 2012; 21(6): 937-947.

12. Zhao X, Liu L, Li X, Zeng J, Jia X, Liu P. Biocompatible graphene oxide nanoparticle-based drug delivery platform for tumor microenvironment-responsive triggered release of doxorubicin. Langmuir. 2014; 30(34): 10419-10429.

13. Zhu S, Meng Q, Wang L, Zhang J, Song Y, Jin H, et al. Highly photoluminescent carbon dots for multicolor patterning, sensors, and bioimaging. Angewandte Chemie. 2013; 125(14): 4045-4049.

14. Shen J, Zhu Y, Yang X, Li C. Graphene quantum dots: emergent nanolights for bioimaging, sensors, catalysis and photovoltaic devices. Chemical communications. 2012; 48(31): 3686-3699.

15. Chen M L, He Y J, Chen X W, Wang J H. Quantum-dot-conjugated graphene as a probe for simultaneous cancer-targeted fluorescent imaging, tracking, and monitoring drug delivery. Bioconjugate chemistry. 2013; 24(3): 387-397.

16. Wang C, Wu C, Zhou, X, Han T, Xin X, Wu J, et al. Enhancing cell nucleus accumulation and DNA cleavage activity of anti-cancer drug via graphene quantum dots. Scientific reports. 2013; 3(1): 1-8.

17. Massai D, Isu G, Madeddu D, Cerino G, Falco A, Frati C, et al. A versatile bioreactor for dynamic suspension cell culture. Application to the culture of cancer cell spheroids. PloS one. 2016; 11(5): 154610.

18. Chen J, Chen S, Zhao X, Kuznetsova L V, Wong S S, Ojima I. Functionalized single-walled carbon nanotubes as rationally designed vehicles for tumor-targeted drug delivery. Journal of the American Chemical Society. 2008; 130(49): 16778-16785.

19. Lee H, Mok H, Lee S, Oh Y K, Park T G. Target-specific intracellular delivery of siRNA using degradable hyaluronic acid nanogels. Journal of Controlled Release. 2007; 119(2): 245-252.

20. Platt V M, Szoka JrF C. Anticancer therapeutics: targeting macromolecules and nanocarriers to hyaluronan or CD44, a hyaluronan receptor. Molecular pharmaceutics. 2008; 5(4): 474-486.

21. Qhattal H S S, Liu,X. Characterization of CD44-mediated cancer cell uptake and intracellular distribution of hyaluronan-grafted liposomes. Molecular pharmaceutics. 2011; 8(4): 1233-1246.

22. Chen C, Zhao S, Karnad A, Freeman J W. The biology and role of CD44 in cancer progression: therapeutic implications. Journal of hematolog & oncology. 2011; 11(1): 1-23.

23. Thomas R G, Moon M, Lee S, Jeong Y Y . Paclitaxel loaded hyaluronic acid nanoparticles for targeted cancer therapy: in vitro and in vivo analysis. International journal of biological macromolecules. 2015; 72: 510-518.

24. Lee JE, In I, Lee H, Lee K D, Jeong J H, Park S. Target delivery and cell imaging using hyaluronic acid-functionalized graphene quantum dots. Molecular pharmaceutics. 2013; 10(10): 3736-3744.

25. Kim K, Choi H, Choi E S, Park M H, Ryu J H. Hyaluronic acid-coated nanomedicine for targeted cancer therapy. Pharmaceutics. 2017; 11(7): 301.

26. Nigam P, Waghmode S, Louis M, Wangnoo S, Chavan P, Sarkar D. Graphene quantum dots conjugated albumin nanoparticles for targeted drug delivery and imaging of pancreatic cancer. Journal of Materials Chemistry B. 2014; 2(21): 3190-3195.

27. Zhou Z, Tang J, Sun Q, Murdoch W J, Shen Y. A multifunctional PEG–PLL drug conjugate forming redox-responsive nanoparticles for intracellular drug delivery. Journal of Materials Chemistry B. 2015; 3(38): 7594-7603.

28. Vasir J K, Labhasetwar V. Quantification of the force of nanoparticle-cell membrane interactions and its influence on intracellular trafficking of nanoparticles. Biomaterials. 2008; 29(31): 4244-4252.

29. Ahirwar S, Mallick S, Bahadur D. Electrochemical method to prepare graphene quantum dots and graphene oxide quantum dots. ACS omega. 2017; 2(11): 8343-8353.

30. Zhang X, Li M, Wang Y B, Cheng Y, Zheng Y F, Xi F, et al. Cell response of nanographene platelets to human osteoblast-like MG63 cells. Journal of Biomedical Materials Research Part A. 2014; 102(3): 732-742.

31. Sanghwa J, Pinals R L, Bhushan D, Hayong S, Ankarao K, Debika D, et al. Graphene Quantum Dot Oxidation Governs Noncovalent Biopolymer Adsorption. Scientific Reports (Nature Publisher Group). 2020; 25: 59-56.

32. Iannazzo D, Pistone A, Salamò M, Galvagno S, Romeo R, Giofré S V, et al. Graphene quantum dots for cancer targeted drug delivery. International journal of pharmaceutics. 2017; 518(1-2): 185-192.

33. He H, Feng M, Hu J, Chen C, Wang J, Wang X, et al. Designed short RGD peptides for one-pot aqueous synthesis of integrin-binding CdTe and CdZnTe quantum dots. ACS applied materials & interfaces. 2012; 4(11): 6362-6370.

34. Zheng XT, Than A, Ananthanaraya A, Kim D H, Chen P. Graphene quantum dots as universal fluorophores and their use in revealing regulated trafficking of insulin receptors in adipocytes. ACS nano. 2013; 7(7): 6278-6286.

35. Dong Y, Pang H, Yang H B, Guo C, Shao J, Chi Y, et al. Carbon-based dots co-doped with nitrogen and sulfur for high quantum yield and excitation-independent emission. Angewandte Chemie International Edition. 2013; 52(30): 7800-7804.

36. Skwarek E, Bolbukh Y, Tertykh V, Janusz W. Electrokinetic properties of the pristine and oxidized MWCNT depending on the electrolyte type and concentration. Nanoscale research letters. 2016; 11(1): 1-17.

37. Fan T, Zeng W, Tang W, Yuan C, Tong S, Cai K, et al. Controllable size-selective method to prepare graphene quantum dots from graphene oxide. Nanoscale research letters. 2015; 10(1): 1-8.

38. Zhu S, Song Y, Zhao X, Shao J, Zhang J, Yang B. The photoluminescence mechanism in carbon dots (graphene quantum dots, carbon nanodots, and polymer dots): current state and future perspective. Nano research. 2015; 8(2): 355-381.

39. Wang X, Sun X, Lao J, He H, Cheng T, Wang M, et al. Multifunctional

graphene quantum dots for simultaneous targeted cellular imaging and drug delivery. Colloids and Surfaces B: Biointerfaces. 2014; 122: 638-644.

40. https://pubmed.ncbi.nlm.nih.gov/22216895/

41. Kudin K N, Ozbas B, Schniepp H C, Prud'Homme RK, Aksay I A, Car R. Raman spectra of graphite oxide and functionalized graphene sheets. Nano letters. 2008; 8(1): 36-41.

42. Sobon G, Sotor J, Jagiello J, Kozinski R, Zdrojek M, Holdynski M, et al. Graphene oxide vs. reduced graphene oxide as saturable absorbers for Er-doped passively mode-locked fiber laser. Optics express. 2012; 20(17): 19463-19473.

43. https://pubmed.ncbi.nlm.nih.gov/23712762/

44. Chan F K M, Moriwaki K, De Rosa M J. Detection of necrosis by release of lactate dehydrogenase activity. In Immune Homeostasis. Humana Press, Totowa, NJ. 2013; 12: 26-63.

45. Chen W, Lv G, Hu W, Li D, Chen S, Dai Z. Synthesis and applications of graphene quantum dots: a review. Nanotechnology Reviews. 2018; 7(2): 157-185.

46. Jiang D, Chen Y, Li N, Li W, Wang Z, Zhu J, et al. Synthesis of luminescent graphene quantum dots with high quantum yield and their toxicity study. PLoS ONE. 2015;10(12): 5–7.

47. Ko N R, Nafiujjaman M, Lee J S, Lim H N, Lee Y K, Kwon IK. Graphene quantum dot-based theranostic agents for active targeting of breast cancer. RSC Advances. 2017; 7(19): 11420–11427.